

Are your MRI contrast agents cost-effective?

Learn more about generic Gadolinium-Based Contrast Agents.



FRESENIUS
KABI

caring for life

AJNR

Diagnostic Accuracy of Arterial Spin-Labeling, Dynamic Contrast-Enhanced, and DSC Perfusion Imaging in the Diagnosis of Recurrent High-Grade Gliomas: A Prospective Study

This information is current as of April 19, 2024.










T.B. Nguyen, N. Zakhari, S. Velasco Sandoval, A. Guarnizo-Capera, M. Alexios Gulak, J. Woulfe, G. Jansen, R. Thornhill, N. Majtenyi and G.O. Cron

AJNR Am J Neuroradiol 2023, 44 (2) 134-142

doi: <https://doi.org/10.3174/ajnr.A7771>

<http://www.ajnr.org/content/44/2/134>

Diagnostic Accuracy of Arterial Spin-Labeling, Dynamic Contrast-Enhanced, and DSC Perfusion Imaging in the Diagnosis of Recurrent High-Grade Gliomas: A Prospective Study

 T.B. Nguyen,  N. Zakhari,  S. Velasco Sandoval,  A. Guarnizo-Capera, M. Alexios Gulak,  J. Woulfe,  G. Jansen,  R. Thornhill,  N. Majtenyi, and  G.O. Cron



ABSTRACT

BACKGROUND AND PURPOSE: For patients with high-grade gliomas, the appearance of a new, enhancing lesion after surgery and chemoradiation represents a diagnostic dilemma. We hypothesized that MR perfusion without and with contrast can differentiate tumor recurrence from radiation necrosis.

MATERIALS AND METHODS: In this prospective study, we performed 3 MR perfusion methods: arterial spin-labeling, DSC, and dynamic contrast enhancement. For each lesion, we measured CBF from arterial spin-labeling, uncorrected relative CBV, and leakage-corrected relative CBV from DSC imaging. The volume transfer constant and plasma volume were obtained from dynamic contrast-enhanced imaging without and with T1 mapping using modified Look-Locker inversion recovery (MOLLI). The diagnosis of tumor recurrence or radiation necrosis was determined by either histopathology for patients who underwent re-resection or radiologic follow-up for patients who did not have re-resection.

RESULTS: There were 26 patients with 32 lesions, 19 lesions with tumor recurrence and 13 lesions with radiation necrosis. Compared with radiation necrosis, lesions with tumor recurrence had higher CBF ($P = .033$), leakage-corrected relative CBV ($P = .048$), and plasma volume using MOLLI T1 mapping ($P = .012$). For differentiating tumor recurrence from radiation necrosis, the areas under the curve were 0.81 for CBF, 0.80 for plasma volume using MOLLI T1 mapping, and 0.71 for leakage-corrected relative CBV. A correlation was found between CBF and leakage-corrected relative CBV ($r_s = 0.54$), volume transfer constant, and plasma volume ($0.50 < r_s < 0.77$) but not with uncorrected relative CBV ($r_s = 0.20$, $P = .29$).

CONCLUSIONS: In the differentiation of tumor recurrence from radiation necrosis in a newly enhancing lesion, the diagnostic value of arterial spin-labeling-derived CBF is similar to that of DSC and dynamic contrast-enhancement-derived blood volume.

ABBREVIATIONS: ASL = arterial spin-labeling; AUC = area under the curve; DCE = dynamic contrast-enhanced; k^{trans} = volume transfer constant; MOLLI = modified Look-Locker inversion recovery; pCASL = pseudocontinuous pulse ASL; rCBV = relative CBV (CBV lesion/CBV normal contralateral white matter); ROC = receiver operating characteristic; SI = signal intensity; SMART₁Map = saturation method using adaptive recovery times for cardiac T1 mapping; Vp = plasma volume

In the monitoring of patients with high-grade gliomas treated with standard chemoradiation, the presence of a newly enhancing lesion seen on MR imaging often represents a diagnostic

dilemma. While subjective radiologic assessment of MR imaging contrast-enhancement patterns can be useful for differentiating recurrence from treatment-related effects,¹ there is evidence that quantitative perfusion can improve diagnostic accuracy.^{2,3}

DSC MR imaging is the most widely used perfusion technique in clinical practice. There have been fewer reports on the diagnostic accuracy of other perfusion techniques such as dynamic contrast-enhanced (DCE) MR imaging and arterial spin-labeling (ASL) in differentiating tumor recurrence and treatment-related effects.⁴⁻⁶ Unlike DSC and DCE techniques, ASL does not require any contrast injection and can provide simple quantification of CBF.⁷ While earlier applications of ASL on 1.5T clinical systems had inadequate signal-to-noise, the increased availability of 3T scanners has made the technique suitable for broader clinical translation. Our hypothesis is that ASL can provide diagnostic value similar to that of DSC MR imaging and DCE MR imaging

Received July 28, 2022; accepted after revision December 30.

From the Department of Radiology (T.B.N., N.Z., R.T.), Radiation Oncology and Medical Physics, and Department of Pathology and Laboratory Medicine (J.W., G.J.), The Ottawa Hospital, Ottawa, Ontario, Canada; University of Ottawa (T.B.N., N.Z., J.W., G.J., R.T.), Ottawa, Ontario, Canada; The Ottawa Hospital Research Institute (T.B.N., J.W., G.J., R.T.), Ottawa, Ontario, Canada; Division of Neuroradiology (S.V.S., A.G.-C.), Department of Radiology, Hospital Universitario Fundación Santa Fe de Bogotá, Bogotá, D.C., Colombia; Department of Anesthesiology and Pain Medicine (M.A.G.), University of Toronto, Toronto, Ontario, Canada; Department of Medical Physics (N.M.), Grand River Regional Cancer Centre, Kitchener, Ontario, Canada; and Stanford University (G.O.C.), Stanford, California.

Grant support was provided by GE Healthcare for this researcher-initiated study.

Please address correspondence to Thanh B. Nguyen, MD, Department of Radiology, The Ottawa Hospital, Civic Campus, 1053 Carling Ave, Room J1115, Ottawa, ON, K1Y 4E9, Canada; e-mail: thnguyen@toh.ca

<http://dx.doi.org/10.3174/ajnr.A7771>

in the characterization of a newly enhancing lesion seen in patients with treated high-grade gliomas. Our primary objective was to evaluate the diagnostic accuracy of ASL, DCE MR imaging, and DSC MR imaging in the differentiation of recurrent tumor from treatment-related changes in patients with treated high-grade gliomas. A secondary objective was to compare different methods of T1 mapping for DCE MR imaging.

MATERIALS AND METHODS

Study Population

This study was approved by the local ethics board (REB#20160425-01H, The Ottawa Hospital). Written informed consent was obtained from each patient enrolled in this study. Patients who presented with a newly enhancing lesion suspicious for a recurrent glioma between December 2017 and November 2021 at our hospital were prospectively enrolled. We included adult patients (18 years of age or older) who developed a new parenchymal enhancing lesion on follow-up MR imaging after receiving standard treatment. Treatment was based on the Stupp Protocol and consisted of surgical resection followed by standard radiation treatment with concomitant temozolomide. Patients were excluded for the following reasons: 1) a small enhancing lesion (measuring <1 cm in maximal length); 2) patients who did not have a re-resection and had incomplete radiologic or clinical follow-up following the research MR imaging; 3) delay between MR imaging and the operation (>65 days); and 4) no perfusion imaging or the lesion not covered on perfusion imaging.

Imaging Acquisition

Each patient was scanned on a 3T MR imaging scanner (Discovery MR750W; GE Healthcare). The conventional MR imaging protocol used axial T1 precontrast (TR = 8.1 ms, TE = 3 ms, TI = 450 ms, flip angle = 90°, voxel size = 0.44 × 0.44 × 1 mm); axial T2 FLAIR (TR = 1000 ms, TE = 92 ms, TI = 2651 ms, flip angle = 160°, voxel size = 0.86 × 0.86 × 3 mm); and axial T1 postcontrast (TR = 13 ms, TE = 2.9 ms, flip angle = 12°, voxel size = 1 × 1 × 1 mm). Axial DWI was acquired (multiple b-values from 10 to 1000 s/mm², TR = 5000 ms, TE = 98.9 ms, voxel size = 0.94 × 0.94 × 4.5 mm). ADC maps were generated in-line (on the scanner). Before gadolinium injection, ASL was performed using pseudocontinuous pulse ASL (pCASL) with a 3D stack of fast spin-echo readout (TR = 4588 ms, TE = 10.3 ms, flip angle = 111°, postlabeling delay = 2025 ms, voxel size = 1.8 × 1.8 × 5 mm, number of slices = 16, number of excitations = 3, duration = 4 minutes 13 seconds). Five background suppression (inversion) pulses were used.

For both DCE MR imaging and DSC MR imaging, we used intravenous injections of Gadovist 1.0 (Bayer Schering Pharma). For DCE MR imaging, a fixed dose of 0.05 mmol/kg of Gadovist was injected at 2 mL/s. For DSC MR imaging, a second dose of gadolinium (0.05 mmol/kg) was injected 10 minutes after the first injection at a rate of 4 mL/s. DCE MR imaging was performed using a 3D spoiled gradient-recalled sequence (TR = 5.3 ms, TE = 1.1 ms, flip angle = 25°, voxel size = 1.9 × 2.5 × 5 mm, 80 phases, duration = 4 minutes 35 seconds). For DSC MR imaging, we used a T2*-weighted EPI gradient recalled-echo sequence (TR = 1275 ms, TE = 45 ms, flip angle = 90°, voxel size = 1.8 ×

1.8 × 5 mm, 50 phases, duration = 2 minutes 8 seconds). Two T1-mapping sequences were performed before and after contrast injection for all patients except for the last 10: saturation method by using adaptive recovery times for cardiac T1 mapping (SMART₁Map) (TR = 4.1 ms, TE = 1.6 ms, flip angle = 20°, voxel size = 1.9 × 2.5 × 5 mm, duration = 2 minutes 53 seconds) and modified Look-Locker inversion recovery (MOLLI) (TR = 4.5 ms, TE = 1.6 ms, flip angle = 20°, voxel size = 1.9 × 2.5 × 5 mm, duration = 2 minutes 53 seconds).⁸

Postprocessing of ASL Images

The perfusion-weighted images were produced in-line and were quantified into CBF values via a single compartment model by using the following equation:

$$CBF_{ASL} = 6000 \times \lambda \frac{\left[1 - \exp\left(-\frac{ST(s)}{T1t(s)}\right)\right] \exp\left(\frac{PLD(s)}{T1b(s)}\right)}{2T1b(s) \left[1 - \exp\left(-\frac{LT(s)}{T1b(s)}\right)\right]} \left(\frac{PW}{SF \times PD}\right) \varepsilon \times NEX$$

For this equation, *T1b* is the T1 of blood and is assumed to be 1.6 seconds. The partial saturation of the reference image (*PD*) is corrected for using a *T1t* of 1.2 seconds (typical of gray matter). *ST* is saturation time and is set to 2 seconds. The partition coefficient λ is set to the whole-brain average, 0.9. The efficiency, ε , is a combination of both inversion efficiency (0.8) and background suppression efficiency (0.75), resulting in an overall efficiency of 0.6. *PLD* is the postlabeling delay. *LT* is the labeling duration set to 1.5 seconds. *PW* is the perfusion-weighted or the raw difference image. *SF* is the scaling factor of the *PW* sequence. The CBF is reported in milliliters/100 g/minute. *NEX* is the number of excitations for *PW* images.

Postprocessing of DSC Images

DSC images were processed using singular value decomposition and deconvolution as implemented in a commercially available software package (Olea Sphere 3.0; Olea Medical). MR signal intensity was converted to a T2* relaxation rate. An automated algorithm selected the most suitable pixels for the vascular input function. The signal intensity (SI) was converted to relative change in R2* using the standard expression: $\Delta R2^*(t) = -\ln[S(t) / S_0] / TE$, where *S* is the SI at time *t*; *S*₀, the baseline SI; and *TE*, the echo time. Correction for leakage in CBV calculations was done using a pre-injection of contrast agent from the DCE acquisition and linear fitting to estimate the T1 contamination caused by extravasation of contrast agent. Both uncorrected and corrected CBV maps were generated.

Postprocessing of DCE Images

Three methods were used to process the DCE images: 1) without T1 correction, 2) T1 correction with a SMART₁Map acquisition, and 3) T1 correction with MOLLI acquisitions. The extended Tofts model was used in all cases. For all patients, DCE images were processed directly in the software (Olea Sphere 3.0) to generate maps of plasma volume (*Vp*) and volume transfer constant (*K^{trans}*). The SI was converted to percentage change in signal intensity (relSI) using the expression: $relSI(t) = 100 \times [S(t) - S_0] / S_0$

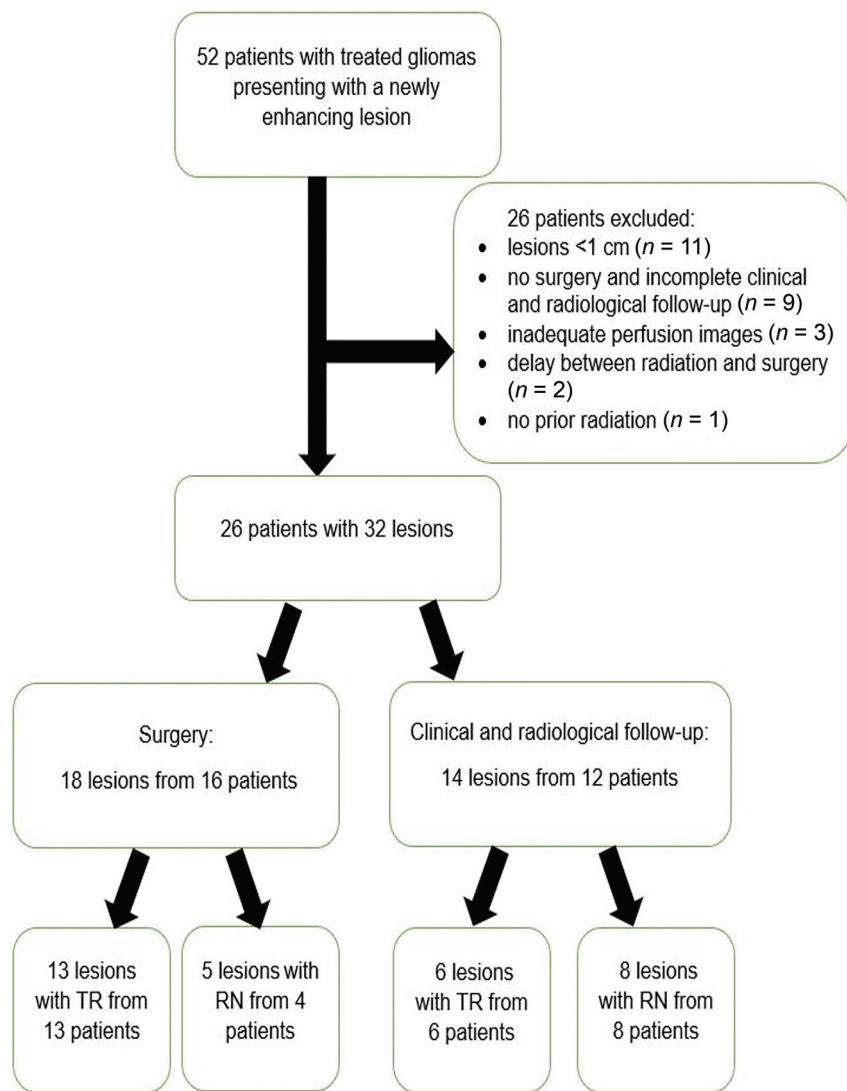


FIG 1. Flow chart of patients included and excluded in the study. Among the 26 patients included in the study, 6 patients had 2 lesions, 2 patients had 1 lesion with tumor recurrence (TR) and 1 lesion with radiation necrosis (RN), both confirmed with clinical/radiologic follow-up; 1 patient with 2 lesions with RN confirmed with surgery; 1 patient had 1 lesion with TR and 1 lesion with RN confirmed with surgery; 1 patient with 1 lesion with TR confirmed by surgery and 1 lesion with RN confirmed with clinical/radiology follow-up; 1 patient had 1 lesion with TR confirmed with surgery and 1 lesion with TR confirmed with clinical/radiologic follow-up.

where S is the SI at time t and S_0 is the baseline SI. The vascular input function was selected from a small ROI placed in the superior sagittal sinus directly from the DCE images. Signal conversion was set as SI to $\text{relSI}(\%)$. For patients who also had T1 mapping, the SI-versus-time curve was converted to gadolinium-versus-time using the T1 maps obtained before and after contrast from either the SMART₁Map or MOLLI acquisitions. This bookend T1 mapping has been described elsewhere.⁹ V_p and K^{trans} were then calculated for both T1-mapping techniques using the same Olea Sphere software.

Image Interpretation

A senior neuroradiologist trained a senior neuroradiology fellow on ROI placement and verified the technique. For each patient,

the fellow, who was blinded to the outcome, drew an ROI over the largest solid component of the newly enhancing lesion using axial T1-weighted postcontrast images avoiding adjacent vessels and cystic, necrotic, or hemorrhagic areas. This ROI was coregistered on all the other parametric maps. For the uncorrected CBV and corrected CBV maps, an additional ROI was placed in the contralateral unaffected white matter to obtain a ratio (normalized value). The mean value for each ROI on each parametric map was recorded.

Reference Standard

For patients who underwent resection of the newly enhancing lesions, a neuropathologist blinded to the imaging results assessed the presence and percentage of viable tumor and/or radiation necrosis in the surgical specimens. Visual assessment was performed under $\times 4$ high-power-field microscopy to determine the approximate percentage area of radiation necrosis or tumor recurrence relative to the whole-tissue area on all available slides. The following criteria were used for the diagnosis of radiation necrosis: the presence of coagulative necrosis and hyalinized vessels. For the diagnosis of recurrent tumor, we used the following criteria: the presence of increased cellularity and nuclear pleomorphism. In lesions in which there was a mixture of viable tumor and radiation necrosis, a lesion was categorized as tumor recurrence if the percentage of viable tumor was higher than the percentage of radiation necrosis.

For patients who did not undergo an operation, clinical and radiologic

follow-up following the research MR imaging was used to classify the lesion as radiation necrosis or tumor recurrence. Two neuroradiologists, blinded to the perfusion analysis, assessed the change in the morphology and size of the enhancing lesion on the follow-up MR imaging using conventional and diffusion-weighted sequences. The presence of a centrally restricted diffusion pattern in an enhancing lesion was found to be associated with a treatment-related effect.¹⁰ Thus, our criteria for tumor recurrence were the following: 1) presence of a nodular or solid component that progressively increases in size with time; and 2) absence of restricted diffusion in the central area of necrosis on visual assessment of the $b = 1000$ images and the ADC map. Criteria for radiation necrosis were the following: 1) a peripheral rim of enhancement that remains stable or

Table 1: Clinical and characteristics of patient population^a

	Radiation Necrosis	Tumor Recurrence	P Value
Median age (yr) (95% CI)	54 (44–63.2)	59 (50.9–65.3)	.34
Female/male	13% (1/12)	21% (4/15)	.35
Initial tumor grade: grade 3, grade 4	0, 13	4, 15	.098
Median duration from radiation treatment to study MR imaging (days), (95% CI)	179 (142–462)	275 (191–915)	.066
% Lesions with resection	30% (5/13)	68% (13/19)	.27
Median duration from imaging to resection (days) (95% CI)	20	15 (13.5–26)	.96
Median Karnofsky score (range)	80 (75.3–90)	80 (70–90)	.43

^a Patients with 2 lesions are entered as 2 separate entries for the purpose of this table.

Table 2: Comparison of perfusion parameters for lesions diagnosed as tumor recurrence versus radiation necrosis

	Radiation Necrosis			Tumor Recurrence			P Value
	No.	Median	95% CI	No.	Median	95% CI	
CBF_AS_L (mL/100 g/min)	13	24.1	17.8–38.3	19	36.0	33.9–62.2	.003 ^a
rCBV	13	1.81	1.55–3.18	19	3.69	2.02–5.03	.058
Corrected rCBV	13	1.24	0.83–2.89	19	2.50	1.60–3.15	.048
K ^{trans} _SI (min ⁻¹)	13	0.013	0.0062–0.039	19	0.019	0.011–0.048	.28
Vp_SI	13	0.16	0.12–0.29	19	0.27	0.21–0.39	.063
K ^{trans} _MOLLI (min ⁻¹)	11	0.052	0.024–0.094	14	0.055	0.047–0.11	.44
Vp_MOLLI	11	0.17	0.13–0.28	14	0.28	0.20–0.41	.012
K ^{trans} _SMART (min ⁻¹)	11	0.042	0.020–0.075	14	0.046	0.037–0.071	.48
Vp_SMART	11	0.12	0.082–0.23	14	0.21	0.15–0.33	.080

^a Significance following Holm Bonferroni correction.

decreases in size, or 2) the presence of a central area of restricted diffusion on visual assessment of the $b = 1000$ images and the ADC map. The 2 neuroradiologists agreed on the classification of 12 of 14 lesions. Consensus reading was obtained for the remaining 2 lesions.

Statistical Analysis

For each lesion, the spatial coefficient of variation for each perfusion parameter was calculated as the SD of the parameter divided by the mean value of the parameter within the tumor ROI.¹¹

For certain continuous clinical variables (such as age and duration between MR imaging and the operation) and for each perfusion parameter, differences between the 2 patient groups were assessed via Mann-Whitney U tests. While P values $< \alpha = .05$ were considered statistically significant, a stepwise Holm Bonferroni procedure was applied to minimize the potential for type I errors due to multiple comparisons.¹² Associations between variables were investigated using the Spearman coefficients of rank correlation. Associations with coefficients of >0.8 were considered very strong; between 0.60 and 0.79, strong; between 0.40 and 0.59, moderate; and <0.39 , weak. Receiver operator characteristic (ROC) curves were constructed for each variable and the area under each ROC was evaluated. Both the standard error of the area under each ROC curve and comparisons between areas under each ROC curve were evaluated using the method of DeLong et al.¹³ All data were analyzed using MedCalc (Version 12; MedCalc Software).

RESULTS

There were 52 patients who were prospectively enrolled in this study. We excluded the following patients: one patient had a recurrence but did not have prior radiation ($n = 1$); 2 patients had resection >3 months after the MR imaging ($n = 2$); 11 patients

had a newly enhancing lesion measuring <1 cm in maximal length ($n = 11$); 9 patients did not have resection and had short clinical and radiologic follow-up of <3 months duration ($n = 9$); and 3 patients were missing one of the perfusion imaging sequences ($n = 1$) or had perfusion imaging that did not cover the lesion ($n = 2$) (Fig 1). The clinical and demographic information for these 26 patients is listed in Table 1. In the final analysis, there were 32 lesions, with 6 patients having 2 lesions. Histopathology was obtained for 18 lesions with 13 lesions categorized as tumor recurrence (7 lesions with mixed pathology but a higher proportion of tumor and 6 lesions with only tumor) and 5 lesions categorized as radiation necrosis (3 lesions with mixed pathology but a higher proportion of radiation necrosis and 2 lesions with pure radiation necrosis). Clinical and radiologic follow-up was used to assess the outcome of 14 lesions (6 tumor recurrence, 8 radiation necrosis).

The mean area for the lesion ROI was 350.1 (SD, 263.6) mm². The mean area for the contralateral normal white matter was 34 (SD, 6.7) mm². For the 32 lesions, the mean spatial coefficient of variation for the ASL_perfusion-weighted values was 27.4%, which was lower than those derived from Vp_MOLLI (57.6%), Vp_SMART (60%), Vp_SI (53.8%), CBV (90.2%), and corrected CBV (70%).

For ASL perfusion imaging, the median CBF value was lower for patients with radiation necrosis (24.1 mL/100 g/min; 95% CI, 17.8–38.3 mL/100 g/min) compared with those with tumor recurrence (36.0 mL/100 g/min; 95% CI, 33.9–62.2 mL/100 g/min) (Table 2). For DSC perfusion imaging, the median corrected relative CBV (rCBV) was also lower for patients with radiation necrosis (1.24; 95% CI, 0.83–2.89) compared with patients with tumor recurrence (2.50; 95% CI, 1.60–3.15). There was a trend toward lower median uncorrected rCBV for patients with radiation necrosis (1.81; 95% CI, 1.55–3.18) compared with patients with

Table 3: Correlogram between different perfusion parameters using the Spearman rank correlation coefficient^a

	CBF_ASL (ml/100g/min)	rCBV	Corrected rCBV	Ktrans_SI (min ⁻¹)	Vp_SI	Ktrans_MOLLI (min ⁻¹)	Vp_MOLLI	Ktrans_SMART (min ⁻¹)	Vp_SMART
CBF_ASL (ml/100g/min)		0.195	0.542	0.503	0.581	0.633	0.769	0.655	0.593
rCBV	0.195		0.478	0.061	0.225	0.088	0.078	0.128	0.081
Corrected rCBV	0.542	0.478		0.286	0.552	0.441	0.642	0.476	0.549
Ktrans_SI (min ⁻¹)	0.503	0.061	0.286		0.784	0.829	0.594	0.788	0.394
Vp_SI	0.581	0.225	0.552	0.784		0.523	0.728	0.531	0.618
Ktrans_MOLLI (min ⁻¹)	0.633	0.088	0.441	0.829	0.523		0.636	0.981	0.506
Vp_MOLLI	0.769	0.078	0.642	0.594	0.728	0.636		0.653	0.766
Ktrans_SMART (min ⁻¹)	0.655	0.128	0.476	0.788	0.531	0.981	0.653		0.595
Vp_SMART	0.593	0.476	0.549	0.394	0.618	0.506	0.766	0.595	

^a Color coding is red for a very strong correlation ($r_s > 0.8$); orange for a strong correlation ($0.6 \leq r_s \leq 0.79$), yellow for a moderate correlation ($0.4 \leq r_s \leq 0.59$), and green for a weak correlation ($r_s < 0.4$).

tumor recurrence (3.69; 95% CI, 2.02–5.03) ($P = .058$). For DCE imaging, Vp_SI and K^{trans}_{SI} (derived from percentage change in signal intensity without T1 mapping) were not statistically significantly different between the 2 groups ($P = .063$ and $P = .28$, respectively, Table 2). For the subgroup of patients who underwent T1 mapping with either MOLLI or SMART₁Map sequences, exploratory analysis of 25 lesions (11 radiation necrosis and 14 tumor recurrence) revealed that Vp_MOLLI (derived from MOLLI T1 mapping) was lower for radiation necrosis than for tumor recurrence (0.17; 95% CI, 0.13–0.28 versus 0.28; 95% CI, 0.20–0.41). Vp_SMART (derived from SMART₁Map mapping), K^{trans}_{SMART} , and K^{trans}_{MOLLI} were not statistically significant between the 2 groups ($P = .08$, $P = .48$, and $P = .44$, respectively). Following the Holm Bonferroni stepwise correction for multiple comparisons ($n = 9$), CBF_ASL was the only perfusion parameter that remained statistically significantly different between the 2 groups ($P < .0055$).

The correlation between CBF_ASL and Vp_MOLLI was very strong ($r_s = 0.77$, $P < .001$, Table 3). Correlations between CBF_ASL and other DCE parameters (K^{trans}_{MOLLI} , K^{trans}_{SI} ,

K^{trans}_{SMART} , Vp_SI, and Vp_SMART) were moderate-to-strong (r_s between 0.50 and 0.66, $P \leq .004$). There was a moderate correlation between CBF_ASL and the corrected CBV ratio ($r_s = 0.54$, $P = .001$). Only a weak and insignificant correlation was found between CBF_ASL and the uncorrected CBV ratio ($r_s = 0.20$, $P = .29$).

In the differentiation between radiation necrosis and tumor recurrence, the diagnostic accuracy for CBF_ASL was good (AUC = 0.81; 95% CI, 0.64–0.98, Table 4). By means of the criterion of CBF > 30 mL/100 g/min, sensitivity was 0.84 (95% CI, 0.62–0.97) and specificity was 0.77 (95% CI, 0.46–0.95). Among the three lesions which were misclassified as false negatives with ASL, one case was likely due to ineffective labeling, because the CBF was lower in the entire right cerebral hemisphere compared with the left (Fig 2).

Compared with ASL-derived CBF, the diagnostic accuracies for uncorrected rCBV (AUC = 0.70; 95% CI, 0.52–0.89) and corrected rCBV (AUC = 0.71; 95% CI, 0.51–0.90, Table 4) were slightly lower, though these differences did not reach statistical significance ($P = .4$ and $P = .30$, respectively). By means of the

Table 4: Diagnostic accuracy of various parameters in the differentiation between tumor recurrence and radiation necrosis for all lesions (n = 32 lesions) and for subgroup analysis of patients with DCE T1 mapping (n = 25 lesions)^a

Parameters	No.	AUC (95% CI)	P Value	Optimal Threshold	Sensitivity (%)	Specificity (%)
ASL_CBF	32	0.81 (0.63–0.93)	<.001	>30 mL/100 g/min	84 (60–97)	77 (46–95)
rCBV	32	0.70 (0.52–0.89)	.033	>2.43	69 (43–87)	77 (46–95)
Corrected rCBV	32	0.71 (0.51–0.90)	.037	>1.54	79 (54–94)	69 (39–91)
$K^{\text{trans}}_{\text{SI}}$	32	0.61 (0.41–0.82)	.27	>0.0093 (min ⁻¹)	84 (60–97)	46 (19–75)
Vp_SI	32	0.69 (0.51–0.88)	.038	>0.18	79 (54–94)	62 (32–86)
$K^{\text{trans}}_{\text{SI}}$	25	0.66 (0.43–0.88)	.17	>0.0092 (min ⁻¹)	86 (57–98)	55 (23–83)
Vp_SI	25	0.68 (0.46–0.90)	.10	>0.18	79 (49–95)	64 (31–89)
$K^{\text{trans}}_{\text{MOLLI}}$	25	0.59 (0.36–0.82)	.44	>0.045 (min ⁻¹)	78 (49–95)	45 (17–77)
Vp_MOLLI	25	0.80 (0.62–0.98)	<.001	>0.19	86 (57–98)	63 (31–89)
$K^{\text{trans}}_{\text{SMART}}$	25	0.58 (0.34–0.83)	.49	>0.024 (min ⁻¹)	92 (66–1)	27 (6–61)
Vp_SMART	25	0.71 (0.49–0.88)	.057	>0.12	93 (66–1)	54 (23–83)

^aStatistics are listed with their 95% CI.

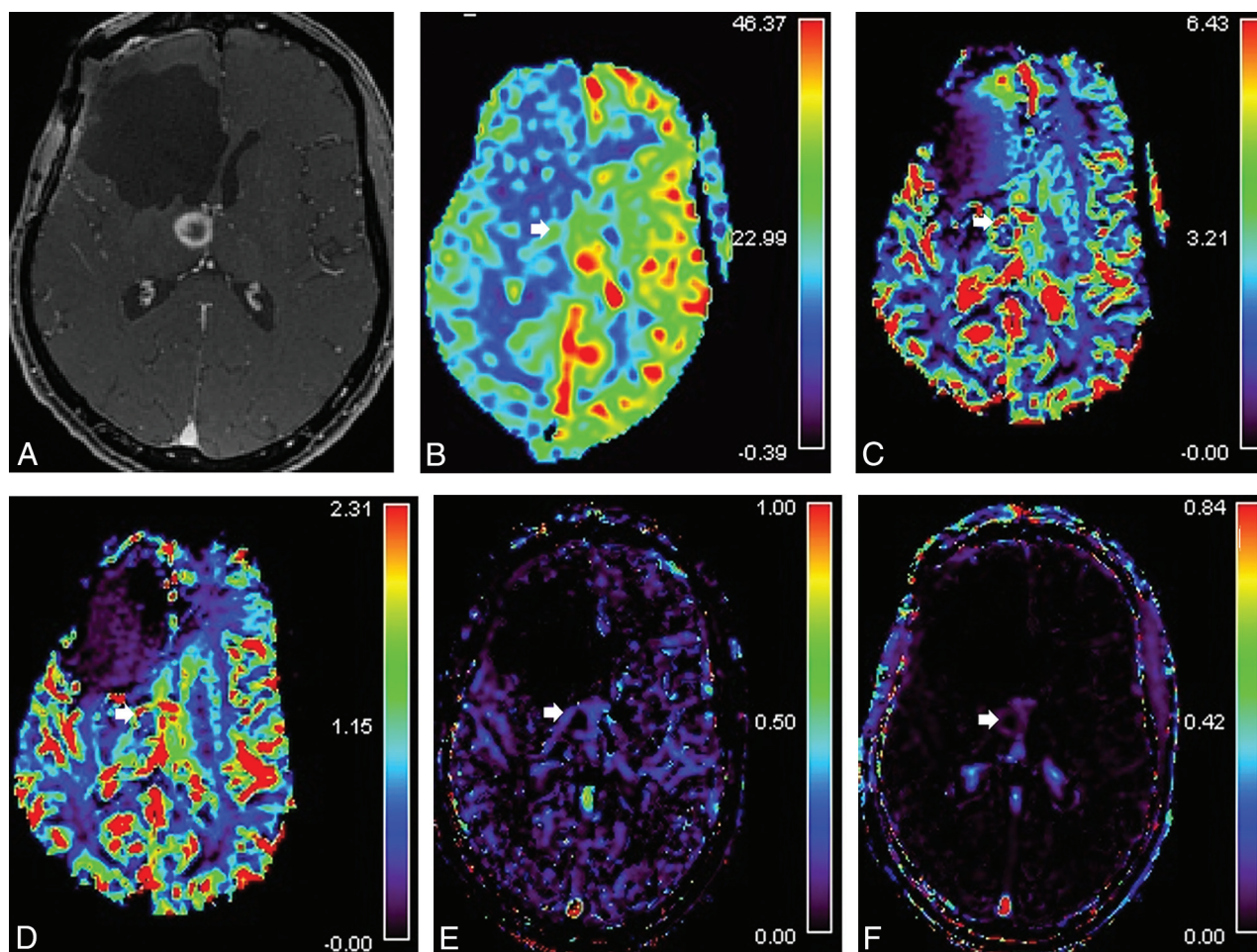


FIG 2. Sample of a case of recurrent glioblastoma multiforme with a false-negative ASL study due to probable ineffective labeling. Patient had a history of a right frontal grade IV glioma and had undergone resection and chemoradiation 3 years earlier. A, Axial T1-weighted image shows a newly enhancing lesion in the right anterior thalamus. B, ASL-derived CBF reveals a low CBF value in the enhancing lesion (arrow). The CBF in the right hemispheric cortex is lower than on the left side, presumably due to ineffective labeling from dental hardware. DSC MR imaging demonstrates a high, uncorrected rCBV value (C) and leakage-corrected rCBV value (D) at the rim of the enhancing lesion (arrow). DCE MR imaging using MOLLI T1 mapping shows high Vp (E) and K^{trans} (F) values in the lesion (arrows). Pathology confirmed glioblastoma recurrence.

criterion of rCBV > 2.43, sensitivity was 0.69 (95% CI, 0.43–0.87) and specificity was 0.77 (95% CI, 0.46–0.95). By means of the criterion of corrected rCBV > 1.54, sensitivity was 0.79 (95% CI, 0.54–0.94) and specificity was 0.69 (95% CI, 0.39–0.91). Among the 4 patients with false-negative findings, 1 patient had a right temporal lesion that was obscured by susceptibility artifacts on

the CBV map from DSC but was correctly identified on the CBF map from ASL and DCE MR imaging (Fig 3).

For patients who underwent DCE imaging with T1 mapping, Vp derived from MOLLI had the best diagnostic accuracy (AUC = 0.80; 95% CI, 0.62–0.98), which was statistically higher than that of $K^{\text{trans}}_{\text{MOLLI}}$ (AUC = 0.59; 95% CI, 0.36–0.82)

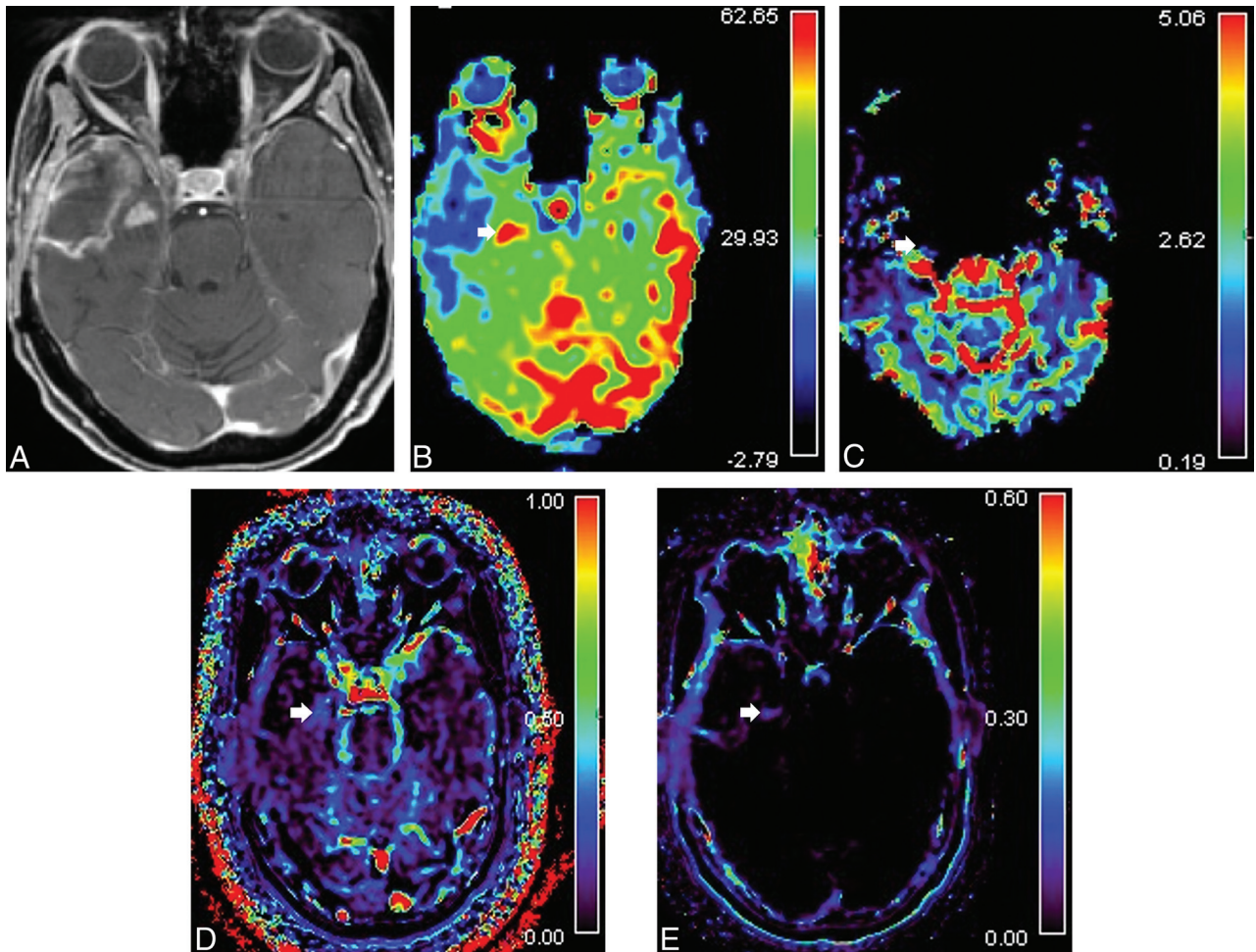


FIG 3. Example of a case of recurrent glioblastoma multiforme with a false-negative DSC study due to susceptibility artifacts. *A*, Axial T1-weighted image shows a newly enhancing lesion in the right mesial temporal lobe. *B*, ASL-derived CBF map demonstrates a marked increase in CBF in the lesion (*arrow*). *C*, Corrected CBV map is unreliable in the tumoral region due to susceptibility artifacts (*arrow*). DCE MR imaging performed without T1 mapping reveals high V_p (*D*) and K^{trans} (*E*) values in the lesion (*arrow*), which correlate with the high CBF value.

and K^{trans}_{SMART} (AUC = 0.58; 95% CI, 0.34–0.83) ($P = .04$ and $P = .035$, respectively). The diagnostic accuracy of V_p_{SI} (AUC = 0.68; 95% CI, 0.46–0.90), V_p_{SMART} (AUC = 0.71; 95% CI, 0.49–0.88), and K^{trans}_{SI} (AUC = 0.66; 95% CI, 0.43–0.88) was lower than that for V_p_{MOLLI} , though this did not reach statistical significance ($P > .05$). Using a criterion of $V_p_{MOLLI} > 0.19$, sensitivity was 0.86 (95% CI, 0.57–0.98) and specificity was 0.63 (95% CI, 0.31–0.89).

DISCUSSION

The results of this prospective study suggest that ASL-derived CBF measurements offer a degree of accuracy similar to that of DSC-derived CBV measurements in differentiating tumor recurrence and radiation necrosis. Our results are in line with those of prior studies published in the literature. A meta-analysis by Wang et al³ revealed a pooled sensitivity of 79% and specificity of 78% for ASL. Two other studies not included in that meta-analysis reported sensitivities of 92% and 100% and specificities of 93% and 88%.^{14,15} Manning et al¹⁴ reported that 6 lesions located near the skull base were correctly identified by ASL but were misclassified by DSC MR imaging because of susceptibility artifacts. We

had 1 such patient in our study in whom the tumor was misclassified by DSC because of susceptibility artifacts due to the temporal bone but was correctly identified by ASL. However, ASL perfusion might also be affected by susceptibility artifacts at the skull base or in the neck, which can cause poor labeling. There was 1 patient with a thalamic lesion that was misclassified on ASL due to probable poor labeling but correctly identified on CBV derived from DSC. Thus, differences in the reported diagnostic accuracy of ASL and DSC imaging in the literature might be influenced by the inclusion or exclusion of cases with susceptibility artifacts in the study. Use of ASL perfusion has many advantages in the clinical workflow: absence of gadolinium injection, reasonable acquisition time (<5 minutes), relative standardization of the acquisition methods, and minimal postprocessing time. A consensus article by the International Society of Magnetic Resonance in Medicine perfusion study group and the European Consortium for ASL in Dementia recommended the use of a 3D multiecho segmented readout scheme with the pCASL labeling method on a 3T MR imaging scanner. CBF maps are usually calculated directly from the MR imaging console without the need for additional off-line postprocessing and are immediately sent to the PACS for clinical review.

In the differentiation between tumor recurrence and radiation necrosis using DCE imaging, we have found that plasma volume was more accurate than K^{trans} . A systematic review and meta-analysis found that K^{trans} had a pooled sensitivity of 0.75 and specificity of 0.79 in the diagnosis of tumor recurrence versus treatment-related changes.¹⁶ However, some authors have reported lower sensitivities for K^{trans} (0.62 and 0.51, respectively), which are in agreement with our study.^{17,18} Bolcaen et al¹⁹ found higher wash-in and washout rates on the dynamic contrast-enhancement curves in rats with glioblastoma versus those with radiation necrosis, but no difference in K^{trans} was found between the 2 groups. They believed that K^{trans} measurements in their study could have been biased because the commercial software performed a voxel-by-voxel analysis for each parameter, which can introduce more noise than performing the calculation on a number of pixels inside a specific ROI.

Our study suggests that the diagnostic accuracy of Vp in the differentiation of glioma recurrence from radiation necrosis can be improved with the use of a T1-mapping technique, such as the Look Locker method, compared with a method that does not use any T1 mapping. Current recommendations by Quantitative Imaging Biomarkers MRI Biomarker Committee suggest the use of a variable flip angle technique for T1 mapping, which is more readily available than the MOLLI sequence. However, the MOLLI technique might offer higher reproducibility than the variable flip angle technique.²⁰ Alternatively, a model-independent analysis based on the integration of the signal intensity curve across time as proposed by Hamilton et al²¹ could provide diagnostic accuracy similar to that of more complex model-dependent analysis, which requires T1 mapping.

A major limitation of our study is the small sample size, which might not have allowed us to detect a statistical difference in the diagnostic accuracy between ASL and DSC/DCE imaging. A second limitation is the lack of direct spatial correlation between the ROI measurements on perfusion maps with histopathologic findings. There is a risk of misclassification because the ROI might not match the resected area. In our study, we tried to mitigate this risk by obtaining an ROI over the entire enhancing lesion rather than a small hot-spot ROI within the enhancing lesion because most of the enhancing lesion was usually resected at surgery and sent to pathology at our institution.

CONCLUSIONS

In patients with high-grade gliomas who developed a newly enhancing lesion following standard chemoradiation treatment, the accuracy of ASL-derived CBF is similar to that of DSC and DCE-derived blood volume for the differentiation of tumor recurrence from radiation necrosis.

Disclosure forms provided by the authors are available with the full text and PDF of this article at www.ajnr.org.

REFERENCES

- Mullins ME, Barest GD, Schaefer PW, et al. Radiation necrosis versus glioma recurrence: conventional MR imaging clues to diagnosis. *AJNR Am J Neuroradiol* 2005;26:1967–72 [Medline](#)
- van Dijken BR, van Laar PJ, Holtman GA, et al. Diagnostic accuracy of magnetic resonance imaging techniques for treatment

- response evaluation in patients with high-grade glioma: a systematic review and meta-analysis. *Eur Radiol* 2017;27:4129–44 [CrossRef Medline](#)
- Wang L, Wei L, Wang J, et al. Evaluation of perfusion MRI value for tumor progression assessment after glioma radiotherapy: a systematic review and meta-analysis. *Medicine (Baltimore)* 2020;99:e23766 [CrossRef Medline](#)
- Wang YL, Chen S, Xiao HF, et al. Differentiation between radiation-induced brain injury and glioma recurrence using 3D pCASL and dynamic susceptibility contrast-enhanced perfusion-weighted imaging. *Radiother Oncol* 2018;129:68–74 [CrossRef Medline](#)
- Choi YJ, Kim HS, Jahng GH, et al. Pseudoprogression in patients with glioblastoma: added value of arterial spin labeling to dynamic susceptibility contrast perfusion MR imaging. *Acta Radiol* 2013;54:448–54 [CrossRef Medline](#)
- Ozsunar Y, Mullins ME, Kwong K, et al. Glioma recurrence versus radiation necrosis? A pilot comparison of arterial spin-labeled, dynamic susceptibility contrast enhanced MRI, and FDG-PET imaging. *Acad Radiol* 2010;17:282–90 [CrossRef Medline](#)
- Alsop DC, Detre JA, Golay X, et al. Recommended implementation of arterial spin-labeled perfusion MRI for clinical applications: a consensus of the ISMRM perfusion study group and the European consortium for ASL in dementia. *Magn Reson Med* 2015;73:102–16 [CrossRef Medline](#)
- Cron G, Gulak MA, Majtenyi N, et al. MOLLI versus SMART1 mapping for quantitative brain tumor DCE MRI on a 3T GE 750w: initial experience. In: *Proceedings of the Annual Meeting and Exhibition of the International Society of Magnetic Resonance in Medicine*, Montreal, Quebec, Canada. May 16, 2019 (abstract 2903)
- Foottit C, Cron GO, Hogan MJ, et al. Determination of the venous output function from MR signal phase: feasibility for quantitative DCE-MRI in human brain. *Magn Reson Med* 2010;63:772–81 [CrossRef Medline](#)
- Zakhari N, Taccone MS, Torres C, et al. Diagnostic accuracy of centrally restricted diffusion in the differentiation of treatment-related necrosis from tumor recurrence in high-grade gliomas. *AJNR Am J Neuroradiol* 2018;39:260–64 [CrossRef Medline](#)
- Mutsaerts HJ, Petr J, Václavů L, et al. The spatial coefficient of variation in arterial spin labeling cerebral blood flow images. *J Cereb Blood Flow Metab* 2017;37:3184–92 [CrossRef Medline](#)
- Holm S. A simple sequentially rejective multiple test procedure. *Scandinavian Journal of Statistics* 1979;6:65–70
- DeLong ER, DeLong DM, Clarke-Pearson DL. Comparing the areas under two or more correlated receiver operating characteristic curves: a nonparametric approach. *Biometrics* 1988;44:837–45 [CrossRef Medline](#)
- Manning P, Daghighi S, Rajaratnam MK, et al. Differentiation of progressive disease from pseudoprogression using 3D PCASL and DSC perfusion MRI in patients with glioblastoma. *J Neurooncol* 2020;147:681–90 [CrossRef Medline](#)
- Jovanovic M, Radenkovic S, Stosic-Opincal T, et al. Differentiation between progression and pseudoprogression by arterial spin labeling MRI in patients with glioblastoma multiforme. *J BUON* 2017;22:1061–67 [Medline](#)
- Okuchi S, Rojas-Garcia A, Ulyte A, et al. Diagnostic accuracy of dynamic contrast-enhanced perfusion MRI in stratifying gliomas: a systematic review and meta-analysis. *Cancer Med* 2019;8:5564–73 [CrossRef Medline](#)
- Seeger A, Braun C, Skardelly M, et al. Comparison of three different MR perfusion techniques and MR spectroscopy for multiparametric assessment in distinguishing recurrent high-grade gliomas from stable disease. *Acad Radiol* 2013;20:1557–65 [CrossRef Medline](#)
- Zakhari N, Taccone MS, Torres CH, et al. Prospective comparative diagnostic accuracy evaluation of dynamic contrast-enhanced (DCE) vs. dynamic susceptibility contrast (DSC) MR perfusion in differentiating

- tumor recurrence from radiation necrosis in treated high-grade gliomas. *J Magn Reson Imaging* 2019;50:573–82 [CrossRef Medline](#)
19. Bolcaen J, Descamps B, Acou M, et al. **In vivo DCE-MRI for the discrimination between glioblastoma and radiation necrosis in rats.** *Mol Imaging Biol* 2017;19:857–66 [CrossRef Medline](#)
20. Bane O, Hectors SJ, Wagner M, et al. **Accuracy, repeatability, and interplatform reproducibility of T₁ quantification methods used for DCE-MRI: results from a multicenter phantom study.** *Magn Reson Med* 2018;79:2564–75 [CrossRef Medline](#)
21. Hamilton JD, Lin J, Ison C, et al. **Dynamic contrast-enhanced perfusion processing for neuroradiologists: model-dependent analysis may not be necessary for determining recurrent high-grade glioma versus treatment effect.** *AJNR Am J Neuroradiol* 2015;36:686–93 [CrossRef Medline](#)